Linear Control Compensator for a Variable-Transformer in Wide-Voltage Power Converters

Diego Bernal Cobaleda[1], Fanghao Tian[1], Camilo Suarez[1],Miguel Vivert[2], Wilmar Martinez[1]
1 Dept of Electrical Engineering (ESAT), KU Leuven-Energyville, Diepenbeek-Genk, Belgium
2 Facultad de ciencias aplicadas (FICA), Universidad técnica del norte-IKERGUNE AIE, Ibarra, Ecuador-San Sebastian, Spain
E-mail: diego.bernal,fanghao.tian,camilo.suarez,wilmar.martinez@kuleuven.be - mevivert@utn.edu.ec

***Abstract*—This work presents the design and simulation of a controllable magnetic device. The device can help the Dual Active Bridge converter (DAB) to operate in the soft switching region for wide-load applications. The control law is based on the modification of the ferrite-core's permeance for Variable-Transformers (VT). The frecuency-domain's model of the VT control leg is obtained using the Gyrator-Capacitor theory. Finally, this model is found by the premise that the interactions of the transformer's main fluxes are minimum in the control leg, furthermore this paper also proposed a ferrite-core construction that reduces these interactions, therefore the induced voltage in the control winding is also minimized, meaning the parallel interactions of the fluxes are reduced. The results shows that the perturbations are manageable for the control scheme and do not affect the device operation.**

***Index Terms*—Gyrator-Capacitor, Non-Linear Control, Linear Control, Variable-Transformer, Controllable Magnetics**

I. Introduction

Wide-voltage and wide-power applications are active research areas in the field of power electronics. Usually, power converters are not able to keep high efficiency when they are forced to work at lower voltage or load levels than the nominal ones [1] [2]. Several alternatives have been proposed being the multilevel converters one of the most popular. This solution is characterized by the ability to turn off and on power cells to supply and vary either voltage or current [3]. However, when the variations required are wide, more cells and control signals are required, making the converter implementation complex. An alternative proposed for full-bridge based DC/DC converters considers the use of variable inductors (VI) and or VT. With these devices, the converter gain can be modified by controlling the magnetic flux densities in the inductor or transformer cores. E.g. authors in [4] propose an LLC-DCDC converter that is able to change its voltage gain modifying the leakage inductance of the transformer employing a VI. Following this approach, some researchers have studied how to model and control the magnetic flux. References [5] and [6] have in common that they modify the reluctance or the permeance of the magnetic device by means of saturating regions of the core. With this saturation the flux is altered in the surrounding area, changing the response of the magnetic device. An alternative to this method is shown by the authors in [7] where a mechanical variation of the air gap in the device results in a variation of the magnetic flux density inside the core. Based on the first alternative (electrically controlled magnetic device) this paper models the permeance of the magnetic core, employing the gyrator-capacitor technique. Changes in the magnetic device are achieved by local core saturation by means of a DC-current and an auxiliary winding.

The Gyrator-Capacitor is not a novel technique and arose as a response to linear reluctance model for magnetic materials, Fig. 1 shows this representation; when a current i is applied to an inductor L a voltage v is induced in the winding depending on the amount of turns N. Following this, the gyrator makes the bridge between the electrical space to the magnetic space, where the behaviour of the inductance is modeled as a non-linear permeance, following the electrical-capacitance model. As the capacitance follows a differential equation, the LaPlace domain and the gyrator-capacitor can be used together for designing the control law [8] and as this permeance is implemented in a non-linear form [9] the inductor saturation can be modeled properly. It worth mentioned that this model do not use the flux Φ as the current equivalent but the rate of change of the flux $\dot{\Phi}$.

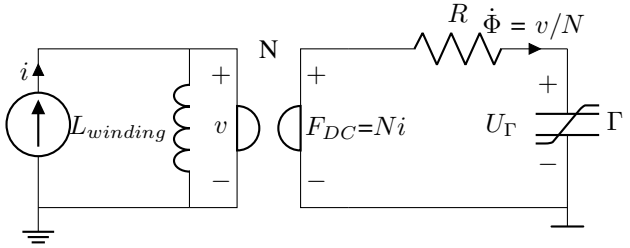

Fig. 1: Gyrator Capacitor representation

As there is no information in the literature that relates a VT with a Dual-Active-Bridge (DAB), in this paper the model proposed by the authors in [10] is modified and implemented using the small signal model of the DAB proposed in [11]. In this application the VT is intended to improve the efficiency of a DAB converter working in a wide range of voltages and loads, as it contributes to compensating the output voltage

variations by modifying the converter's transformer equivalent turns ratio keeping a soft switching operation.

This paper is divided as follow: Section II described how the plant-model was found, In section III the proposed ferrite core is depicted and simulated using finite elements simulation to determine the magnitude of the interaction and how the VT helps the DAB to improve its efficiency for wide load operations, Section IV shows the proposed and designed control architecture, in Section V the simulation results are shown, finally conclusions and future work are presented.

II. Plant Modeling

As mentioned before, a VT can be achieved by modifying the flux path, saturating regions of the core. To take these regions to saturation, an additional magnetic flux needs to be generated. Depending on how the vector sum between the auxiliary flux and the main transformers flux interacts, the technique adopts a different biasing method name.

A. Proposed scenario and physical ferrite structure

Authors in [12]- [15] explain the different types of biasing, and how they influence the variable magnetic device. Fig. 2 shows a graphical representation of the different biasing methods.

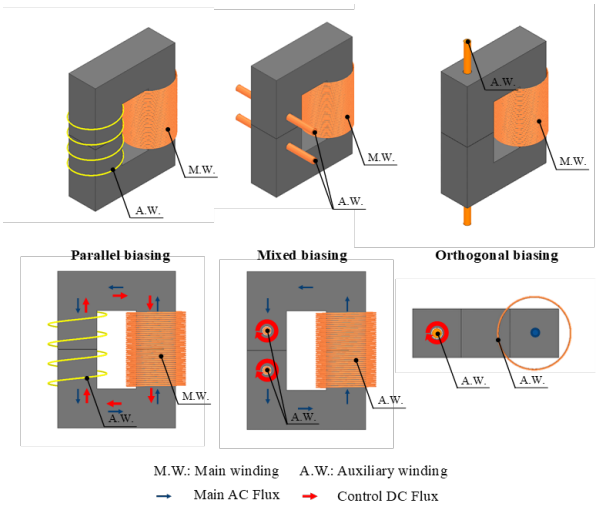

Fig. 2: Flux interaction for different biasing methods in a variable magnetic device

In parallel biasing the auxiliary winding is wound in the same flux path as the main winding, this generates a DC-flux that moves the same direction of the main flux. However for the mixed and orthogonal biasing, orthogonal vector components are presented; for orthogonal biasing, the auxiliary winding is introduced from the top and the flux spins around it, with this, the auxiliary DC-flux-vectors are fully orthogonal to the main flux. Finally for the mixed biasing, the DC-flux interacts in some regions orthogonally and in other regions in parallel. This article assumes that the fluxes are mainly orthogonal, which helps in the accuracy of the small signal modeling as the main transformer flux does no affects the input of the controller.

Fig. 3a shows the isotropic view of the ferrite construction proposed by the authors. As the variations in the main flux are neglected for this application, the circuit in the red box can be analyzed separately from the circuit in the blue box.

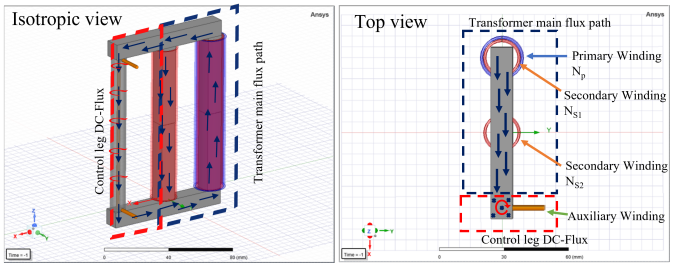

(a) Isotropic view

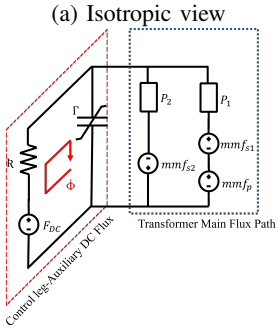

(b) Permeance model

Fig. 3: Transformers topology proposed

For the right side of the blue-boxed circuit, two winding are wound, the first one is the primary winding which can be model as a magneto-motive force (MMF) equals to mmf_p, on the same leg the first part of the secondary winding is wound an can be modeled as mmf_{s1} This secondary winding is divided in two. The second part can be seen in the middle leg of the core, and can also be modeled as a MMF equals to mmf_{s2}. Additionally the dimensions of the core gives to every leg an equivalent permance P_1 and P_2. The equivalent circuit is depicted in Fig. 3b.

Combining the Gyrator-Capacitor depicted in Fig. 1 and expression(1) (Permeance Γ according to [10]) the variables can be explained as: F_{DC} is the input of the system or MMF of the control winding, R represents the losses of the system due to air-gaps, Γ is the permeance of the core, U_Γ the MMF across the permeance Γ, finally, the constans a and n are constanst that depends mainly on the behaviour of the material of the core, and are estimated from the datasheets plots [9] [10].

$$\Gamma = \frac{\Gamma_o}{1 + an|aU_\Gamma|^{n-1}} \tag{1}$$

As for this application the F_{DC} is always positive the MMF of the permeance U_Γ is bigger than 0 as well. Furthermore, a is also greater than 0, thus the absolute value can be neglected.

With these additional constraints, (1) can be written as follow in (2).

$$\Gamma = \frac{\Gamma_o}{1 + an(aU_\Gamma)^{n-1}} \tag{2}$$

By finding the mesh equations in Fig. 1 U_Γ follows the expression shown next.

$$\Gamma \dot{U_\Gamma} = \frac{F_{DC} - U_\Gamma}{R} = \dot{\Phi} \tag{3}$$

B. Change of variable

However, (3) does not give a meaningful control variable, as the system is solved for the MMF. This paper focuses on controlling the permeance, so a change of variable for the equations is proposed. With this modification, the system is changed from $\dot{U} = f(U, F_{DC})$ to $\dot{\Gamma} = g(\Gamma, F_{DC})$. (2) can be written by solving it in terms of Γ as follow

$$U_\Gamma = \frac{(\frac{\Gamma_o - \Gamma}{an\Gamma})^{\frac{1}{n-1}}}{a} \tag{4}$$

Also (2) is derived, $\dot{\Gamma}$ is shown next.

$$\dot{\Gamma} = \dot{U_\Gamma} \frac{2an\Gamma_o U_\Gamma^{n-1}}{(a^2 n U_\Gamma^n + U_\Gamma)^2} \tag{5}$$

Finally merging the expressions (3) $\rightarrow$ (5) and (4) $\rightarrow$ (5) is

$$\dot{\Gamma} = (\frac{F_{DC} - (\frac{(\frac{\Gamma_o - \Gamma}{an\Gamma})^{\frac{1}{n-1}}}{a})}{R\Gamma}) \frac{2an\Gamma_o (\frac{(\frac{\Gamma_o - \Gamma}{an\Gamma})^{\frac{1}{n-1}}}{a})^{n-1}}{(a^2 n (\frac{(\frac{\Gamma_o - \Gamma}{an\Gamma})^{\frac{1}{n-1}}}{a})^n + U)^2} \tag{6}$$

III. Finite Elements Validation

In this section the the proposed core in Fig. 3 is simulated using finite elements technique, the results show how the main flux interacts with the control biasing method, and determines the fluctuations of the auxiliary winding permeance.

A. 3D model simulation

Using Maxwell-Ansys the magnitude of the interactions are plotted in Fig. 4. It can be observed that the DC-flux is concentrated in the control winding and does not spread through the rest of the core, and that the main flux also stays in between the primary and secondary leg.

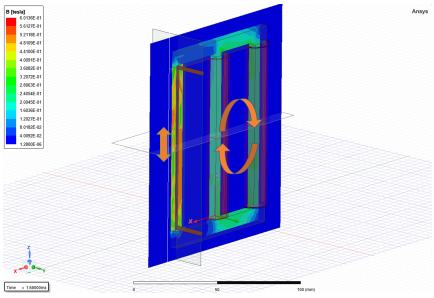

Fig. 4: Auxiliary winding saturation

Additionally in Fig. 5a can also be appreciated that the interactions are not fully orthogonal, as it still exists parallel components in the flux. However, the orthogonal component is bigger in magnitude. Additionally in Fig. 5b the inductance of the control winding is depicted. As the number of turns of this winding is equals to 1, the permeance value depends only in the number of turns of the small signal model shown in the next section. These variations needs to be contemplated in the control scheme. The variations are the result of having in the primary and secondary windings an square voltage of 100V at $50kHz$.

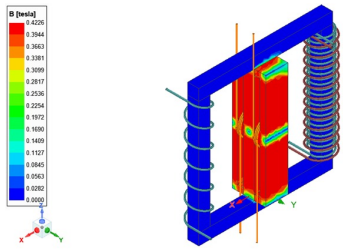

(a) Vector interactions

(b) Control leg permeance variations

Fig. 5: Auxiliary winding open-loop simulation results

B. Dual active bridge soft switching region

The control scheme helps the DAB to modify the output power by means of keeping the equivalent turns ration with unity gain. With this relation, the converter can work in soft-switching region (SSR), improving the efficiency of the system for wide load applications. A small signal model of the transformer shown in Fig. 3b is presented next, the equations are shown in TABLE I. The model is proposed in [11] and is used to determine the Leakage inductance L_{lk}, the magnetizing inductance L_{mag} and the equivalent turns ratio n_{eq} according to the variations on the control variable reluctance $\Re_v$.

Inductances $L_{\Re_1}, L_{\Re_2}, L_{\Re_v}$ are related to the previous mentioned permances P_1, P_2, Γ_o respectively, as the model in [11] is reflected to the primary side, the permeances needs to be multiplied by the second power of the number of turns in the primary winding $n_p^2 P_i$=$L_{\Re_i}$.

With the variations shown in Fig. 5b and the small signal model, the oscillations due to non-orthogonal fluxes coming from the primary and secondary winding, vary from $160\mu[H]$ - $130\mu[H]$ which is translated to $0.15\mu[H*turns]$ - $0.12\mu[H*turns]$ According to these values, the n_{eq} is around 2.5, and the variations in the permeance $\Delta\Gamma = 20\%$.

TABLE I: Transformer small-signal-model according to [11]

$L_{lk} = L_p(1-k^2)$	L_{mag}=$L_p k^2$
$n_{eq} = \frac{nL_{mp}}{k^2 L_p}$	$k = \sqrt{1-\frac{L_{p(ss)}}{L_p}}$
$m = \frac{n_{s_2}}{n_{s_1}}$	$n = \frac{n_{s_1}+n_{s_2}}{n_p}$
$L_p = \frac{(L_{\Re_2}+L_{\Re_v})L_{\Re_1}}{(L_{\Re_2}+L_{\Re_v})+L_{\Re_1}}$	
$L_{mp} = \frac{L_p}{n}(\frac{n_{s_1}}{n_p} - L_{\Re_2}\frac{n_{s_2}}{n_p(L_{\Re_2}+L_{\Re_v})})$	
$L_{p(ss)} = \frac{L_{\Re_1}L_{\Re_2}L_{\Re_v}m^2}{L_{\Re_1}L_{\Re_2}+L_{\Re_1}L_{\Re_v}-2L_{\Re_1}L_{\Re_2}m+L_{\Re_1}L_{\Re_2}m^2+L_{\Re_2}L_{\Re_v}m^2}$	

IV. Linearization and Control Design

As $\dot{\Gamma}$ is a non-linear space state equation a linear model is required. Fig. 6 shows a snapshot from the datasheet of material PC-95 of TDK. With these plots, assuming the core will have an increased temperature, parameters a and n are found. Also the slope of the plot gives information about the maximum and minimum relative permeability μ_r, which directly affects the intial permeance of the core Γ_o and the minimum value of the permeance after saturation $\Gamma_m = R + \Gamma_o(U_{\Gamma_{sat}}) \approx R$.

By changing parameter n the plot will have stiffer slope in saturation, and the behaviour of the core when the temperature is increased can be ajusted. It worth mentioned that as for high temperatures, the core slope(in saturation) is stiffer, the core will resemble more the air behaviour, this is helpful as the main flux can be redirect completely addressing changes similar to removing the control leg.

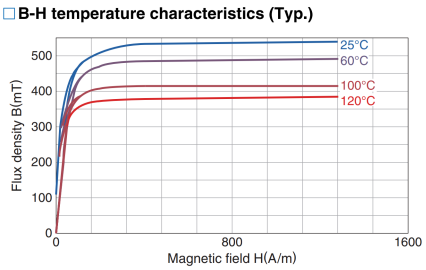

Fig. 6: B vs H of Material PC-95

TABLE II, shows the parameters following the core dimensions and the B vs H curve of the material core.

With the values of TABLE II and the information extracted from the datasheets, (2) is plotted in Fig. 7 to determine the point where the linearization has more robustness.

For this application the controller is more robust when linearized in the second kneee of Fig. 7 due that in this region

TABLE II: Model parameters for Eq.(6)

a	0.6286
n	20
Γ_o	$6.6960x10^{-5}[H*turn]$
Γ_m	$4x10^{-10}[H*turn]$
A_e	$2.0291x10^{-4}[m]$
l_e	$0.0126[m]$
$\Gamma_i, P_i = \frac{\mu_r\mu_o A_e}{l_e}$	

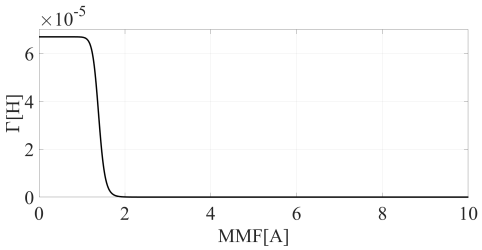

Fig. 7: Γ vs U_Γ According to TABLE II.

μ_r changes from its maximum value, $\Gamma = \Gamma_o$ to saturation $\Gamma \approx R$. (7) shows (6) linearized in $\Gamma_{knee} = 3.38x10^{-7}$ and $U_{knee} = 1.8$.

$$\hat{\dot{\Gamma}} = -0.0012\hat{\Gamma} - 4.1986x10^{-9}\hat{F_{DC}} \tag{7}$$

A. Full-State-feedback-control

As mentioned before, authors in [11] propose a small signal model of a variable transformer. This model is tested using a Dual Active Bridge converter, as the voltages in these type of application depends mainly on Battery levels, the dynamic of the system is considerably slower than the ferrite dynamic response. The rate of change in the voltage determines the speed of the reference, meaning the stabilization of the closed-loop transfer function can be in the order of seconds. With this in mind, the closed-loop poles are chosen in -3.7321 and -0.26795. Following a $\zeta = 2$ and $\omega = 1$.Finally, system (7) is extended to have an integral gain. The controllers constants are shown next. (8) also, shows the augmented matrixes of the system (9)

$$[k_p \; k_i] = \begin{bmatrix} -1.815x10^9 \\ -3.3173x10^9 \end{bmatrix} \tag{8}$$

$$A_{aug} = \begin{bmatrix} -0.0012 & 0 \\ 1 & 0 \end{bmatrix} B_{aug} = \begin{bmatrix} -4.1986x10^{-9} \\ 0 \end{bmatrix} \tag{9}$$

Finally, Fig. 8 depicted the architecture of the controller implemented.

When the voltage in the secondary side of the DAB is shifted by a factor of r a new reference $n_{eq_{ref}} = rn_{eq}$ is generated and solving the equations in TABLE I the permeance reference for the controller is calculated. With this value the DC bias is generated following the linear model and the transformer modified its flux path. In the next section the results of the simulation are shown.

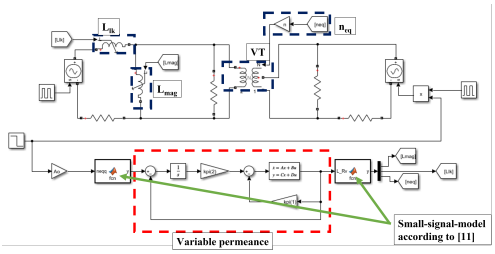

Fig. 8: Control architecture

V. Results

In this section, the implementation of the control scheme in Ansys-Maxwell© is shown. To estimate $\Gamma's$ value the voltage v and current i of the auxiliary winding needs to be measure. Finally as mentioned before, With changes in the DC bus of the secondary side of the DAB a new peremance Γ_{ref}, is calculated using the small signal model in [11]. The DC-current is implemented using an ideal current source. the simulated case of study is shown next in TABLE III. Fig. 9 shows that for the case study the equivalent number of turns, with the control leg unsaturated, is around 2.5, and to get a change of 60% $\Rightarrow n_{eq} = 1.5$ the permeance needs to be changed to $2x10^{-8}[H * turn]$.

TABLE III: Case of study

N	1
p	$4x10^{-10}[H * turn]$
n_{s_1}	65
n_{s_2}	35
n_p	2.5

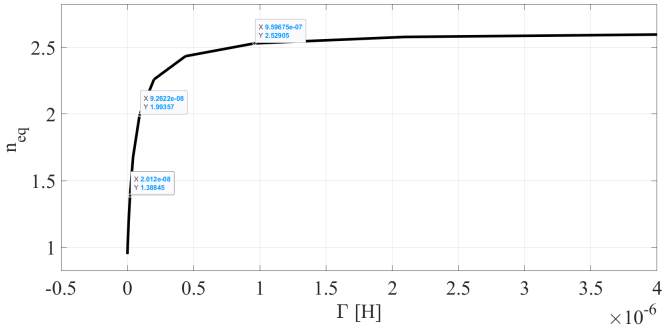

Fig. 9: Modeled equivalent number of turns depending on the permeance of the control leg

It is known that when the DAB voltages are even, the currents are decreased in the transformer improving the efficiency, as when working in soft-switching region, the losses are directly tied to the conduction losses.

In the next section the results of the case of study using a finite-elements simulation environment are shown.

A. Small signal linear model results

In Section III.b oscillations in the permeance of the control winding where presented using finite element simulation results.Fig. 10b shows that these oscillations are strong a noticeable when the leg has 0 current, however, when it is fed by a current of $50[A * turn]$ (calculated using (4)) they decreased considerably. This phenomenon can be explained by observing Fig. 7, where for small currents the permeance value varies easily, however, after saturation the permeance behaves almost constant until it reaches to the permeance of the air. Finally, adding this $\Delta\Gamma$ to the reference of the system Fig. 10a shows the error of the control implementation.

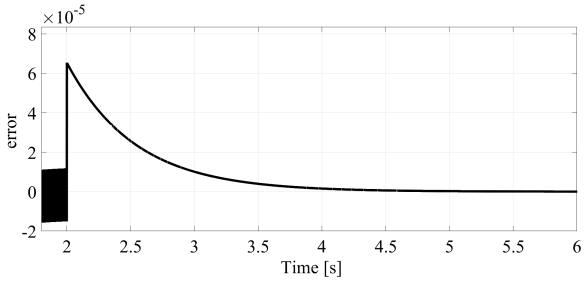

(a) error of the controller

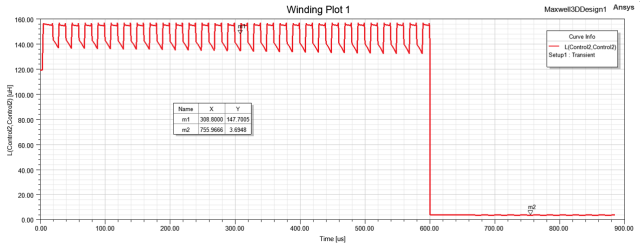

(b) Simulation results of oscillations in the control leg

Fig. 10: Oscillations in the permeance results

Lastly, Fig. 11 shows how the controller, fed by the small signal equations in [11] and by saturating the control leg of the core varies the magnetizing inductance L_{mag}, the leakage inductance L_{lk} and the equivalent turns ration n_{eq}. In the plot can also be observed that L_{mag} fell to a minimum value, even after the other signals stabilize. This effect limits the reflected voltage.

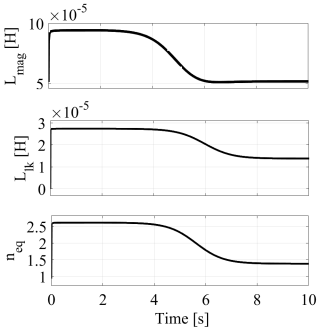

Fig. 11: Variations in the control flux

B. Finite elements large signal simulation results

In this subsection, the core presented in previous sections is fed in three different scenarios according to TABLE III:
1) $v_s = v_p = 100[V]; i_c = 0[A * turn]$
2) $v_s = 100[V]; v_p = 100[V]; i_c = 50[A * turn]$
3) $v_s = 100[V]; v_p = 250[V]; i_c = 0[A * turn]$

Fig. 12 shows $L(Wp, Wp)$,$L(Wp, Wp)$ and $L(Wp, Wp)$ which, by means of the cantilever model are approximated into L_{lkg}, L_{mag} and n_{eq}. The results are sumarized next in TABLE IV

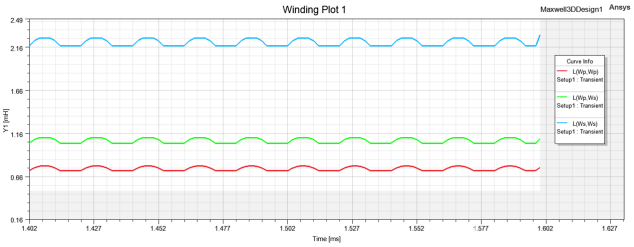

(a) Case: $v_s = v_p = 100[V]; i_c = 0[A * turn]$

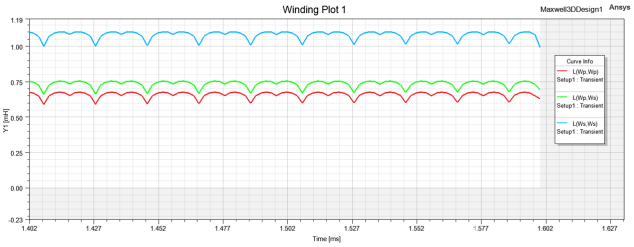

(b) Case: $v_s = v_p = 100[V]; i_c = 50[A * turn]$

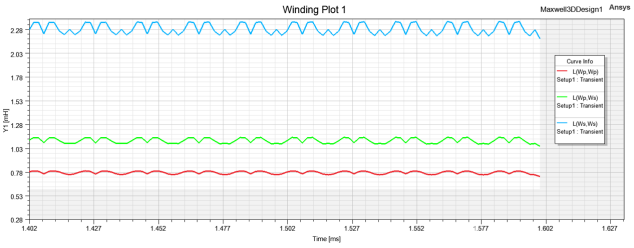

(c) Case: $v_s = 100[V]; v_p = 250[V]; i_c = 0[A * turn]$

Fig. 12: Parasitic inductance variations

Conclusions and Future Work

In this paper, the integration of a small signal model and control technique for a VT in DAB applications is designed and simulated. The simulations show that the equivalent turns ratio can be increased by saturating a magnetic core section by means of the control winding in the VT, this could compensate the reduction of the input voltage and increase the voltage operation of the converter. It can also be observed that the output was not fully compensated, as changes in the Leakage and Magnetizing inductance also happened during the control saturation.

TABLE IV: Model vs Simulation comparison

Parameter	Model	Simulation
$v_s = v_p = 100[V]; i_c = 0[A * turn]$		
L_{lk}	$2.7398e-05$	$239.8x10^{-6}[H]$
L_{mag}	$9.4317e-05$	$520.19x10^{-6}[H]$
n_{eq}	2.6188	2.0377
$v_s = v_p = 100[V]; i_c = 50[A * turn]$		
L_{lk}	$5.4640e-07$	$154.6x10^{-6}[H]$
L_{mag}	$6.0521e-05$	$511.3x10^{-6}[H]$
n_{eq}	0.95	1.4667
$v_s = 100[V]; v_p = 250[V]; i_c = 0[A * turn]$		
L_{lk}	$2.7398e-05$	$219.9x10^{-6}[H]$
L_{mag}	$9.4317e-05$	$560.0x10^{-6}[H]$
n_{eq}	2.6188	2.0177

References

[1] S. Zong, G. Fan and X. Yang, "Double Voltage Rectification Modulation for Bidirectional DC/DC Resonant Converters for Wide Voltage Range Operation," in IEEE Transactions on Power Electronics, vol. 34, no. 7, pp. 6510-6521, July 2019, doi:10.1109/TPEL.2018.2875816.

[2] W. Ye, W. Cui, S. Shao, J. Zhang and K. Sheng, "A Resonant DC-DC Converter with Modular Rectifier for High Voltage Gain and Wide Output Voltage Range Applications," IECON 2019 - 45th Annual Conference of the IEEE Industrial Electronics Society, 2019, pp. 6671-6676, doi:10.1109/IECON.2019.8927312.

[3] X. Yuan, J. Wang, I. Laird and W. Zhou, "Wide-Bandgap Device Enabled Multilevel Converters With Simplified Structures and Capacitor Voltage Balancing Capability," in IEEE Open Journal of Power Electronics, vol. 2, pp. 414-423, 2021, doi: 10.1109/OJPEL.2021.3094713.

[4] Y. Wei, Q. Luo, X. Du, N. Altin, J. M. Alonso and H. A. Mantooth, "Analysis and Design of the LLC Resonant Converter With Variable Inductor Control Based on Time-Domain Analysis," in IEEE Transactions on Industrial Electronics, vol. 67, no. 7, pp. 5432-5443, July 2020, doi: 10.1109/TIE.2019.2934085.

[5] White, Steven & Krause, Thomas & Clapham, Lynann. (2007). Control of flux in magnetic circuits for Barkhausen noise measurements. Measurement Science and Technology. 18. 3501. 10.1088/0957-0233/18/11/034.

[6] M. Enokizono, T. Todaka and T. Yokoyama, "Flux controlling method of magnetic circuit and its application," in IEEE Transactions on Magnetics, vol. 29, no. 6, pp. 3019-3021, Nov. 1993, doi: 10.1109/20.281106.

[7] J. Cui, H. Wang, L. Qu and W. Qiao, "A tunable inductor based on a magnetic flux valve," 2017 IEEE Energy Conversion Congress and Exposition (ECCE), 2017, pp. 3255-3259, doi: 10.1109/ECCE.2017.8096589.

[8] D. C. Hamill, "Gyrator-capacitor modeling: a better way of understanding magnetic components," Proceedings of 1994 IEEE Applied Power Electronics Conference and Exposition - ASPEC'94, 1994, pp. 326-332 vol.1, doi: 10.1109/APEC.1994.316381.

[9] M. Eaton, "Modeling magnetic devices using the gyrator re-cap core model," Proceedings of NORTHCON '94, 1994, pp. 60-66, doi: 10.1109/NORTHC.1994.638970.

[10] Q. Chen, L. Xu, X. Ruan, S. C. Wong and C. K. Tse, "Gyrator-Capacitor Simulation Model of Nonlinear Magnetic Core," 2009 Twenty-Fourth Annual IEEE Applied Power Electronics Conference and Exposition, 2009, pp. 1740-1746, doi: 10.1109/APEC.2009.4802905.

[11] C. Suarez, D. B. Cobaleda and W. Martinez, "Analysis and Validation of Variable Transformers," 2021 IEEE 30th International Symposium on Industrial Electronics (ISIE), 2021, pp. 1-6, doi: 10.1109/ISIE45552.2021.9576416.

[12] J. Pfeiffer, P. Kuster, I. E. M. Schulz, J. Friebe, and P. Zacharias, "Review of Flux Interaction of Differently Aligned Magnetic Fields in Inductors and Transformers," IEEE Access, vol. 9, pp. 2357–2381, 2021.

[13] J. Pfeiffer, P. Kuster, Y. Erenler, Z. H. S. Qashlan, and P. Zacharias, "Impact of implementation of auxiliary bias-windings on controllable inductors for power electronic converters," in 2020 22nd European Conference on Power Electronics and Applications (EPE20 ECCE Europe), 2020.

[14] K. Nakamura, O. Ichinokura, M. Maeda, S. Akatsuka, K. Takasugi, and H. Sato, "Analysis of orthogonal-core type linear variable inductor and

application to VAr compensator," IEEE Trans. Magn., vol. 36, no. 5, pp. 3565–3567, 2000.
[15] O. Ichinokura, K. Nakamura, S. Akatsuka, T. Ohinata, and K. Minazawa, "Development of a Variable Inductor for an Electric Power System," Trans. Magn. Soc. Japan, vol. 5, no. 2, pp. 49–56, 2005.